Theor Chem Acc (2012) 131:1118
DOI 10.1007/s00214-012-1118-x

REGULAR ARTICLE

# Force reversed method for locating transition states

**Keju Sun · Yonghui Zhao · Hai-Yan Su · Wei-Xue Li**

Received: 12 April 2011 / Accepted: 17 August 2011 / Published online: 9 February 2012


**Abstract** To identify the transition state accurately and efficiently on a high-dimensional potential energy surface is one of the most important topics in kinetic studies on chemical reactions. We present here an algorithm to search the transition state by so-called force reversed method, which only requires a rough reaction direction instead of knowing the initial state and final state. Compared to the nudged elastic band method and the dimer method that require multiple images, the present algorithm with only single image required saves significantly the computational cost. The algorithm was implemented in the first-principle periodic total energy calculation package and applied successfully to several prototype surface processes such as the adsorbate diffusion and dissociation on metal surfaces. The results indicate that the force reversed method is efficient, robust to identify the transition state of various surface processes.

**Keywords** Potential energy surface · Force reversed method · Locating transition states

## 1 Introduction

Identification of the transition state (TS) on a high-dimensional potential energy surface (PES) is one of the key issues to understand and control the reaction rate in chemical reactions. However, the complete exploring of the high-dimensional PES is a quite demanding task even with continuous improvement of the computational capability. Various algorithms [1] to locate the transition states without exploring the complete PES are thus developed, such as the methods requiring knowledge of second derivatives of energy (quasi-Newton, trust-region image minimization, quadratic approximation, Cerjan–Miller eigenvector-following etc.) [2–5], some constrained minimization methods with different names [6–10], synchronous transit methods (linear synchronous transit (LST) method and the quadratic synchronous transit (QST) method) [11, 12], the string method [13] (climbing image nudged elastic band (CiNEB) methods [14, 15]), and the dimer method [16].

Though all of these methods aim to find the TS on a high-dimensional PES, the practical implementations are very different, and the efficiency varies and is dependent on PES. Among them, the method requiring knowledge of second derivatives of energy has been successfully applied to small clusters. According to knowledge of second derivatives, one of the local harmonic modes is selected as the searching direction, and the forces on this direction are reversed to locate the TS. However, it becomes inefficient for the calculations of solids and surface of solids because the mode following algorithm scales poorly with size [16]; therefore, it is less used in the periodical calculations. The constrained minimization method is an intuitional method to search the TS; however, it often fails since it follows the slowest ascent path [11, 17, 18]. The synchronous transit method is a fast but crude method, so it normally is used to locate TS with lower precision. The string method particularly the CiNEB method and the dimer method are widely used algorithms to calculate the TS with higher

K. Sun · Y. Zhao · H.-Y. Su · W.-X. Li (✉)
State Key Laboratory of Catalysis, Dalian Institute of Chemical Physics, Chinese Academy of Sciences, Dalian 116023, China
e-mail: wxli@dicp.ac.cn

K. Sun
e-mail: kjsun@dicp.ac.cn

K. Sun · Y. Zhao · H.-Y. Su · W.-X. Li
Dalian Institute of Chemical Physics, Chinese Academy of Sciences, Center for Theoretical and Computational Chemistry, Dalian 116023, China

precision for reactions of solids or reactions on solid surfaces.

Compared to the local minimum searching algorithms, one typically has to provide an initial and tentative reaction coordinate as the searching direction for the algorithms to locate TS. The string method and synchronous transit method generally use the direction pointing from the initial state (IS) to the final state (FS) as the initial searching direction, while the constrained minimization method for instance uses the direction of the interested chemical bond [10]. In the dimer method, the axis of the dimer is used as the searching direction. Although an initial searching direction is not necessary to be provided in principle for the dimer method, it is practically highly desirable, since a good initial searching direction will substantially speed-up the convergence.

Multiple images are required to form a string for CiNEB, whereas two images are required to form a dimer for the dimer method in searching TS. As one can expect, the searching direction guided by the string or dimer through multiply images is time-consuming, and it is desirable to develop the algorithm with single image. In the present work, we describe a simple force reversed method to locate the TS, which requires only one image. Only preliminary and/or rough knowledge about the reaction coordinate is taken as initial searching direction, where no exact reaction direction, the IS and FS is required. In practical implementation, it treats the searching of the TS as locating a local minimum and saves significantly the computational cost. The algorithm proposed is efficient and robust, as demonstrated in various examples in the present work.

## 2 Methods

### 2.1 The primary force reversed (PFR) method

The chemical reactions could be described as a continuous motion on the PES from one local minimum to another along minimum energy path, and the corresponding trajectory is noted as minimum energy path (MEP). The TS is the saddle point with the highest energy along the MEP but in equilibrium for remained freedoms. At a given point not far from the TS, corresponding force $\vec{F}$ could be decomposed to two independent components,

$$\vec{F} = \vec{F}^{//} + \vec{F}^{\perp}, \tag{1}$$

where $\vec{F}^{//}$ is the component paralleled to the reaction coordinate $\vec{R}$ (the direction of the MEP), and $\vec{F}^{\perp}$ is the component perpendicular to $\vec{R}$.

$$\vec{F}^{//} = (\vec{F} \cdot \hat{\vec{R}})\hat{\vec{R}} \tag{2}$$

$$\vec{F}^{\perp} = \vec{F} - \vec{F}^{//}, \tag{3}$$

where $\hat{\vec{R}}$ is the normalized $\vec{R}$,

$$\hat{\vec{R}} = \frac{\vec{R}}{\left|\vec{R}\right|}. \tag{4}$$

In the Cartesian system with $N$ atoms, the paralleled force of the $k$th atom at the direction $q$ ($F^{//}_{k,q}$) is calculated as following

$$F^{//}_{k,q} = \hat{\vec{R}}_{k,q} * \sum_{i=1}^{N}\sum_{q=1}^{3}\left(\vec{F}_{i,q} * \hat{\vec{R}}_{i,q}\right). \tag{5}$$

In the PFR method, the paralleled $\vec{F}^{//}$ is reversed and would point upward along the MEP to the TS. The revised force $\vec{F}^{R}$ on the system becomes therefore

$$\vec{F}^{R} = \vec{F}^{\perp} - \vec{F}^{//} = \vec{F} - 2\vec{F}^{//} \tag{6}$$

If $\vec{F}^{R}$ instead of $\vec{F}$ is used to optimize the system, paralleled component of $\vec{F}^{R}$ would drive the system moving upward along the MEP and perpendicular part optimize the remained freedoms approaching the TS gradually. Given a configuration $\vec{P}_j$ at iteration $j$, the PFR updates to a new configuration

$$\vec{P}_{j+1} = \vec{P}_j + \alpha_j \vec{F}^{R}_j, \tag{7}$$

where $\vec{F}^{R}_j$ is the revised force and $\alpha_j$ is a tunable parameter at iteration $j$. The Eq. 7 defined is the so-called steepest descent method, which is a rather stable and used to illustrate the feature of the PFR method. A more efficient optimizer such as fast inertial relaxation engine [19] could be applied straightforwardly to improve the efficiency further. In this article, to elucidate clearly the advantage of PFR method instead of the optimizer, the steepest descent method and a self-adjusting $\alpha_j$ are used.

$$\alpha_j = 1.5\mathrm{e}^{-\beta_j/2}\alpha_{j-1}, \tag{8}$$

where $\beta_j$ is the arc angle between $\vec{F}^{R}_j$ and $\vec{F}^{R}_{j-1}$. Once the system is fully optimized till all components of $\vec{F}^{R}$ equal to zero, the system will be located exactly at the TS. The searching trajectory will converge directly to the TS if the exact direction of the MEP is known and used as the searching direction by the PFR method. However, in practical implementation, only a rough guessed reaction

direction is known and used as the searching direction, and the convergence varies and may be rather sensitive.

To clarify the influence of the variation between the searching direction and the MEP, we consider following a simplest saddle-shaped PES as an example,

$$E = x^2 - y^2 \tag{9}$$

Obviously, the saddle point (the TS) on this PES is the intersection point of coordinate axes at (0,0) and the MEP is y axes, as shown in Fig. 1. At a given point P, the direction of line $PM'$ (involving $+\overrightarrow{PM}'$ and $-\overrightarrow{PM}'$) is the direction of the MEP, and the direction of line $PM$ (involving $+\overrightarrow{PM}$ and $-\overrightarrow{PM}$) is the guessed reaction direction used as the searching direction. The angle between $PM'$ and $PM$ line is noted as $\theta$ ($0 \leq \theta \leq 90$). When $\theta$ is zero, the guessed reaction direction would be the direction of MEP. Thus, the reversed force $\bar{F}^{R'}$ points right to the TS, and the searching trajectory is a straight line leading directly toward the saddle point (see the black trajectory in Fig. 1). When $\theta$ is not zero, the revised force

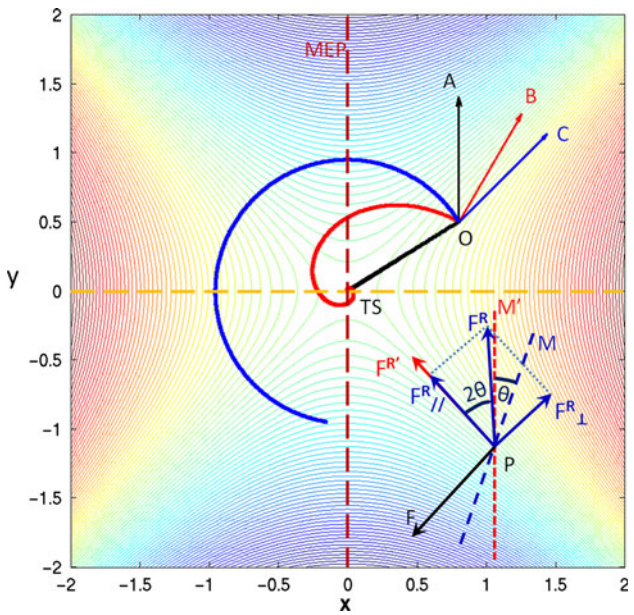


**Fig. 1** (Color on line) The scheme of searching trajectory of the primary force reversed method. $PM'$ is the direction of MEP and $PM$ is the guessed reaction direction, which is used as searching direction. The original force $\vec{F}$, the revised force $\bar{F}^{R'}$ using $PM'$ as searching direction, and the revised force $\bar{F}^{R}$ using $PM$ as the searching direction and its components $\bar{F}^{R}_{//}$ and $\bar{F}^{R}_{\perp}$ at the P point are indicated schematically. Point O is selected randomly as the initial position. *OA* (*black*), *OB* (*red*), and *OC* (*blue*) vectors were selected as the different searching direction, respectively, and corresponding solid lines show the trajectories approaching the TS. The resulted spiral trajectories are indicated

$\bar{F}^{R}$ does not point to TS any more. The angle between $\bar{F}^{R}$ and $\bar{F}^{R'}$ is $2\theta$. $\bar{F}^{R}$ could be decomposed to two independent component, $\bar{F}^{R}_{\perp}$ and $\bar{F}^{R}_{//}$, where $\bar{F}^{R}_{//}$ is the component paralleled to $\bar{F}^{R'}$, and $\bar{F}^{R}_{\perp}$ is the component perpendicular to $\bar{F}^{R'}$. The $\bar{F}^{R}_{//}$ will drive the searching trajectory pointing to the saddle point, and $\bar{F}^{R}_{//}$ will drive the searching trajectory moving around the saddle point. Therefore, the trajectory is a synergetic displacement of pointing toward and moving around the saddle point, which forms a spiral line with the center at the saddle point, accordingly. Since the angle between $\bar{F}^{R}$ and $\bar{F}^{R'}$ is always $2\theta$ for any point on this PES, the spiral line is an equiangular spiral (also named logarithmic spiral or growth spiral). For the saddle-shaped PES with lower symmetry, the trajectory obtained by the PFR method is not a standard equiangular spiral any more but remains an equiangular-like spiral.

When $\theta$ is less than 45° on the PES given by Eq. 9, the trajectory would lead to a convergent spiral line, but when $\theta$ is larger than 45°, the spiral trajectory becomes diverged. When $\theta$ is equal to 45°, the trajectory is a closed circle. Irrespective to the specific angle, the center of the spiral center is always the saddle point. This indicates that the PFR method would approach gradually the TS as long as the angle between the initial searching direction and the direction of the MEP is less than 45°. It should be noted that the restriction of the angle is potential energy surface-dependent, and 45° is only for the potential defined by Eq. 9.

In essence, the PFR method presented here is different from so-called the drag method [6] or similar constrained minimization method. For the drag method, one also needs to choose a reasonable searching direction to drag as in the PFR method. The difference is that the forces in the drag direction are set to zero (fixed) in the drag method, while they are reversed in the PFR method. The revised force $\bar{F}^{R}$ has been applied for structural optimizations until the equilibrium condition is reached, and the TS is identified accordingly. It is clear that only a single DFT calculation with only one image is necessary in the PFR method, which saves significantly the computational cost.

Another difference between the PFR method and the drag method is that the drag method starts from the IS and climbs up along the slowest ascent path, which may be different from the direction of the MEP and may induce the failure to identify the TS [11, 17, 18]. The starting point for the PFR method is, however, flexible in principle and could be any point on PES in the saddle-shape region. Meanwhile, the searching trajectory obtained from the PFR method does not following the slowest ascent direction, and therefore it

could be avoid the failure of the drag method and be more robust. Once the TS is identified, the nearest local minimums at the both sides of TS could be obtained conveniently using the intrinsic reaction coordinates (IRC) approach [20]. Correspondingly, the IS and FS of the elementary reaction as well as the MEP are deducted.

### 2.2 The enhanced force reversed (EFR) method

As indicated in above, for good convergence, the PFR method requires that the angle between the searching direction and the direction of the MEP should be less than a specific value $\theta_s$ (45° for the PES given by Eq. 9). When the angle is close to or larger than $\theta_s$, the convergence will be rather slow or even fail to reach the TS because the equiangular spiral will be divergent. To improve the efficiency and increase the tolerance of $\theta_s$, we propose an enhanced force reversed (EFR) method. We note that the formation of the spiral-like trajectory comes from the deviation ($\theta$) between the searching direction and the direction of the MEP. Therefore, $\theta$ would be in the same direction as the spiral if the direction of $\theta$ is defined as the angle-rotating from searching direction to the direction of the MEP. For example, if the direction of $\theta$ is clockwise, the direction of the spiral is clockwise, and vice versa. Therefore, if one knows the direction of the spiral, the direction of $\theta$ would be known. Then, we could rotate $\vec{R}$ consecutively to decrease $\theta$ and make the searching direction approach to the MEP. Based on the direction variation of two consecutive points on the spiral, the direction of $\theta$ could be obtained. The direction variation of two consecutive points on the spiral is

$$\left( \frac{\vec{F}_j^{\vec{R}_{j-1}}}{\left|\vec{F}_j^{\vec{R}_{j-1}}\right|} - \frac{\vec{F}_{j-1}^{\vec{R}_{j-1}}}{\left|\vec{F}_{j-1}^{\vec{R}_{j-1}}\right|} \right),$$

the searching direction $\vec{R}_{j-1}$ is

$$\left( \frac{\vec{F}_{j-1}^{\vec{R}_{j-1}}}{\left|\vec{F}_{j-1}^{\vec{R}_{j-1}}\right|} - \frac{\vec{F}_{j-1}}{\left|\vec{F}_{j-1}\right|} \right).$$

Therefore, if the new searching direction is assumed to the sum of $\vec{R}_{j-1}$ and direction variation of spiral, $\theta$ could be decreased consistently during the optimization. Therefore, the efficiency of the convergence might be improved, and the tolerance to $\theta_s$ could be enhanced. This could be realized by revising the searching direction $\vec{R}_j$ at iteration $j$ by

$$\vec{R}_j = \left( \frac{\vec{F}_j^{\vec{R}_{j-1}}}{\left|\vec{F}_j^{\vec{R}_{j-1}}\right|} - \frac{\vec{F}_{j-1}}{\left|\vec{F}_{j-1}\right|} \right) \cdot \left|\vec{R}_{j-1}\right|, \tag{10}$$

where $\vec{F}_j^{\vec{R}_{j-1}}$ is the revised force at iteration $j$ using $\vec{R}_{j-1}$ as the searching direction and $\vec{F}_{j-1}$ is the original force at iteration $j-1$.

When the $F_j$ is very small, a small disturbance of force ($\Delta F$) may induce a large change in the direction

$$\left( \Delta \frac{\vec{F}_j^{\vec{R}_{j-1}}}{\left|\vec{F}_j^{\vec{R}_{j-1}}\right|} \right),$$

and accordingly lead to a large variation in $\vec{R}_j$. Then, the number of iterations will increase. Thus, the large change of $\vec{R}_j$ with respect to $\vec{R}_{j-1}$ should be prevented. In the practical implementation, $\vec{R}_j$ is set to $\vec{R}_{j-1}$ if the angle between $\vec{R}_j$ and $\vec{R}_{j-1}$ is larger than 25°. It should be noted that if $\vec{R}_j$ is not limited, the TS still could be exactly located by EFR method with more iterations. Using the EFR method, only limitation for the initial searching direction is that the corresponding angle with respect to the direction of the MEP cannot be 90°, which would rarely occur. This implies that theoretically, the EFR method could reach the TS using a random guessed reaction direction as the searching direction, as long as the guessed reaction direction is not exactly perpendicular to the MEP.

When the EFR method is used to locate the TS, the atoms could be divided into two parts, one part is the reacting atom, which is involved directly in the reaction (such as the oxygen molecule in $O_2$ dissociation on metal surface). The other is the spectator atoms (such as the surface metal atoms in previous example). Since the spectator atoms are not directly involved the reaction, the projection of the searching direction ($\vec{R}$) on them is negligible and set to zero in practical implementation. Therefore, the forces on the reacting atoms ($\vec{R} \neq 0$) will be reversed and used to locate a saddle point following the $\vec{R}$ direction, while the force on the spectator atoms ($\vec{R} = 0$) will be remained (no reversion) to locate a minimum. Because the reacting atoms and the spectator atoms are in

the same system, they are not completely independent. Therefore, the mismatch between them will appear during the process of locating the TS. In most cases, the mismatch will be self-adjusted constantly and vanished when the TS is reached. However, occasionally, the mismatch may be huge and some of the spectator atoms will deviate far away from the equilibrium positions. The deviation will drive the whole PES away from the saddle-shape region, so the EFR algorithm may fail to locate the TS. This happens typically when the initial image is not located in the saddle-shape region of PES. To prevent this happen, one should try to select a different initial image which locates in the saddle-shape region. We present here an alternative method: when the maximum of the forces on the spectator atoms ($F_{\max}(R=0)$) is larger than a critical value (1.5 eV/Å in the article), the EFR will be paused. Accordingly, the searching direction $\vec{R}_j$ and the revised force $\vec{F}^R$ at iteration j are set as following

$$\vec{R}_j = \left( \frac{\vec{F}_j^{\vec{R}_{j-1}}}{\left|\vec{F}_j^{\vec{R}_{j-1}}\right|} - \frac{\vec{F}_{j-1}}{\left|\vec{F}_{j-1}\right|} \right) \cdot \left|\vec{R}_{j-1}\right| \tag{11}$$

$$\vec{F}^R = \vec{F}^{\perp} = \vec{F} - \vec{F}^{//} \tag{12}$$

The whole flow chart of the EFR algorithm is shown in Fig. 2.

Below a number of examples were considered to illustrate the efficiency of the proposed FR algorithm. Either 2-dimension analytic potential surfaces or a first-principle total energy package (Vienna Ab Initio Simulation Package (VASP) [21] in present work) was used to calculate the forces of the interesting systems. For the latter case, electron exchange–correlation interaction was described by generalized gradient approximation in the form of PW91 [22]. VASP uses plane waves to expand wave functions with a cutoff of 400 eV, and PAW potentials [23, 24]. The criteria for the identification of the TS were the residual force less than 0.02 eV $Å^{-1}$. In the present work, the TS was confirmed by the frequency analysis with one and only one imaginary vibration. Once the TS was obtained, the IRC method was applied to find the IS/FS and the corresponding MEP. In this work, the steepest descents method as an IRC approach is used [25]. To test the validity of the FR method, we performed CiNEB calculations to obtain the TS for all the examples using the IS and FS obtained from the IRC approach. Within the numerical error, the calculated TSs (energetics and structures) by CiNEB method are as same as those obtained from the FR method.

Similar to the dimer method, a starting point and an initial searching direction are required to initiate the optimization for the FR method. To elucidate the efficiency of FR method clearly, the number of iterations (the number of gradient evaluations) was compared with the superlinearly converging dimer method [26], a highly efficient and

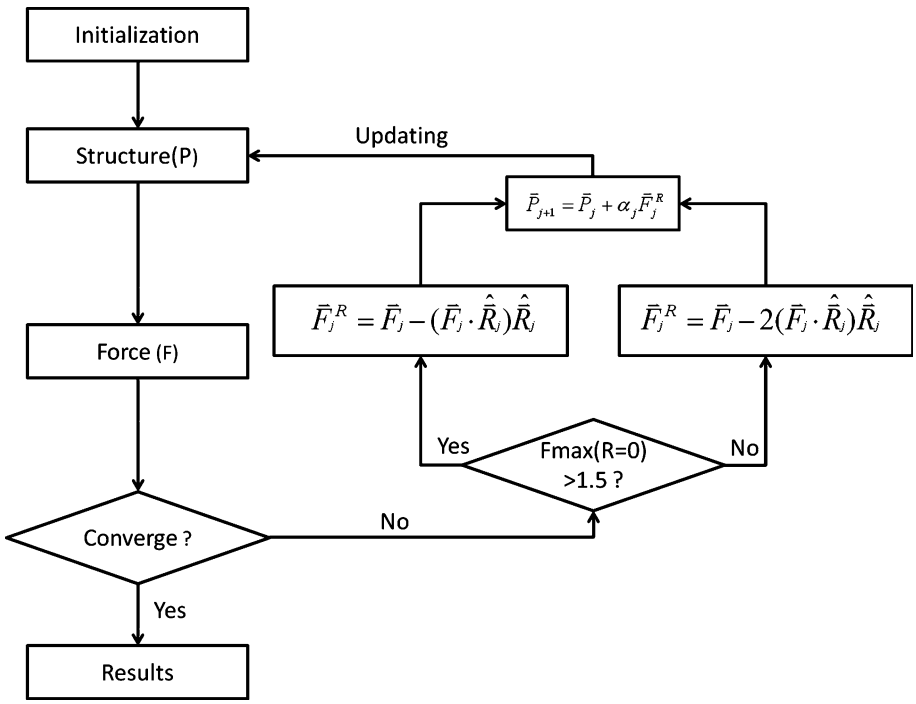


**Fig. 2** Schematic flow chart of the enhanced force reversed method

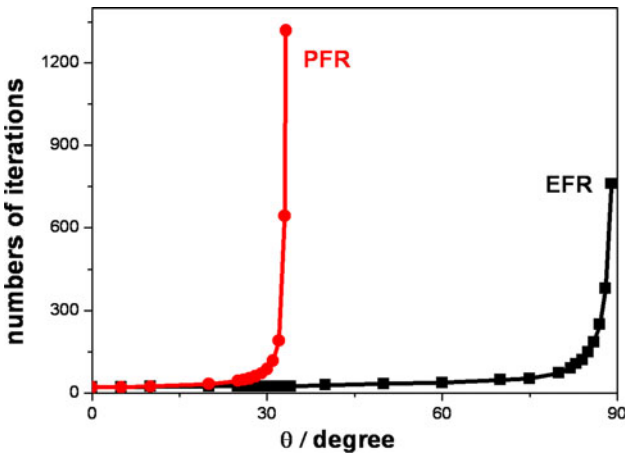


**Fig. 3** (Colored on line) The dependence of number of iterations to locate the TS on the angle $\theta$ (the angle between the initial searching direction and the direction of MEP). The *solid red circle* and *black square* represent the results from the primary force revered method and the enhanced force reversed method, respectively

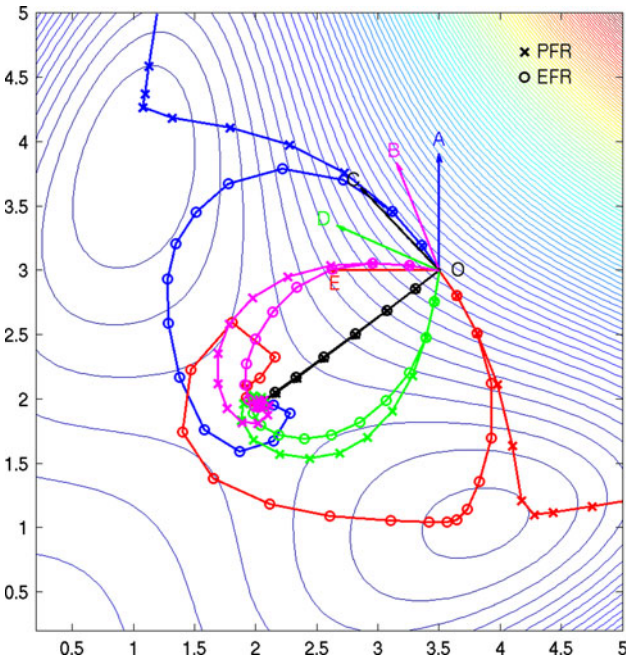


**Fig. 4** (Colored on line) The trajectories to identify the TS on 2D analytic function derived PES (Eq. 13) by the PFR method (represented by "x") and the EFR method (represented by "o"). Starting point O is selected randomly. Five different searching directions *OA*, *OB*, *OC*, *OD,* and *OE* noted with *different colors* are selected. Among of them, *OC* is the one closest to the direction of the MEP

improved dimer method. To make a fair comparison between these two methods, the starting point and the initial searching direction are exact same.

## 3 Results and discussion

To prove that the EFR method is favored over the PFR method in the initial searching direction, we studied the dependence of the two methods on the angle $\theta$, as shown in Fig. 3. The PES is defined by Eq. 9, and the starting point is $(-1,-1)$. $\theta$ is the angle between the initial searching direction and $Y$ axes (the direction of MEP). It is found that there is no pronounced difference between PFR and EFR methods when $\theta$ is less than 20°. Moreover, the number of iterations increases slightly with the increase of $\theta$. When $\theta$ is increased to 30° or even larger, the number of iterations for PFR method increases sharply, whereas the number of iterations for EFR does not increase much until $\theta$ is up to 80°, indicating that the efficiency of EFR is almost independent on $\theta$ in this range. The PFR method will fail to reach the TS, if $\theta$ is larger than 34°. The divergence occurring at 34° instead of theoretical divergent value 45° for given PES originates from the large step length $\alpha$ defined by Eq. 7. When $\theta$ is increased to 89°, the TS can still be reached by EFR method after 760 iterations, which suggests that the range of $\theta$ is widely extended compared to the PFR method.

To further illustrate the efficiency of the FR method, we investigate the TS of a smooth PES derived from a 2D analytic function as indicated in Fig. 4 and given below:

$$E = [(x-y)^2 - 8]^2 + 4(xy-4)^2 + 3x - 2y. \quad (13)$$

In general, if the starting point (O point) is closer to the TS, it is easier and faster to identify the TS. To clarify the robustness and efficiency of the FR algorithm, five different initial searching directions *OA*, *OB*, *OC*, *OD,* and *OE* are selected. As shown in Fig. 4, all five trajectories converge eventually to the TS for the EFR method, while only three of them (*OB*, *OC,* and *OD*) that close to the direction of the MEP converge to TS for the PFR method. The sensitivity on the initial search direction for the PFR method can be clearly seen. It should be noted that the starting point O selected is not close to either the IS or the FS, but actually selected randomly. The convergence to the same TS shows that the proposed FR algorithm, particular the EFR, is flexible and robust. All the trajectories obtained follow neither the MEP nor the slowest ascent path, implying that the FR method is a new method of searching the TS which is different from the NEB methods, the dimer method, or the drag method etc.

To show the difference between the drag method and the FR method explicitly, a well-known PES [17] with two local minima and two TSs is plotted in Fig. 5. The PES has the form of

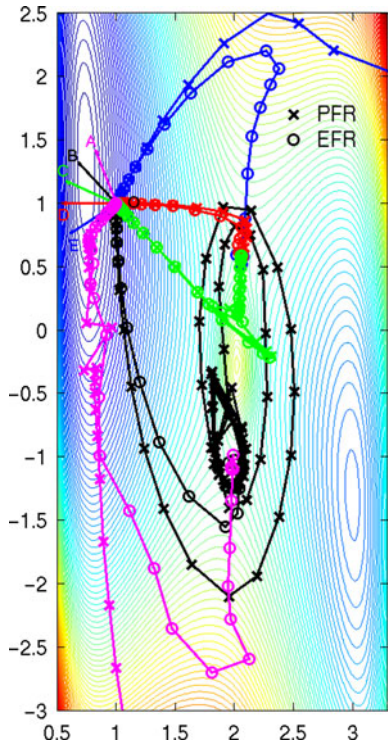


**Fig. 5** (Colored on line) The trajectories of locating the TS on the PES described in [17] with two saddle points by the PFR method (presented by "x") and the EFR method (noted as "o"). Starting point O and five different searching *OA*, *OB*, *OC*, *OD,* and *OE* are indicated

$$\begin{aligned} E = & QQ(4.746,x,0.05)+QQ(4.746,3.742 \\ & -x,0.80)+QQ(3.445,3.742,0.05) \\ & -[JJ(4.746,x,0.05)^2+JJ(4.746,3.742 \\ & -x,0.08)^2+JJ(3.445,3.742,0.05)^2 \\ & -JJ(4.746,x,0.05)JJ(4.746,3.742-x,0.08) \\ & -JJ(4.746,x,0.05)JJ(3.445,3.742,0.05) \\ & -JJ(4.746,3.742-x,0.08)JJ(3.445,3.742,0.05)]^{1/2} \\ & +0.405\left[x-1.871+\frac{y}{1.154}\right]^2 \\ & +1.5\exp\left[-0.5\left(\left(\frac{x-2.02083}{0.1}\right)^2+\left(\frac{y+0.272881}{0.35}\right)^2\right)\right], \end{aligned} \tag{14}$$

where

$$\begin{aligned} & QQ(a,b,c) \\ & =\frac{1.5a\exp[-3.884(b-0.742)]-a\exp[-1.942(b-0.742)]}{2(1+c)} \end{aligned} \tag{15}$$

$$\begin{aligned} & \mathrm{JJ}(a,b,c) \\ & =\frac{a\exp[-3.884(b-0.742)]-6a\exp[-1.942(b-0.742)]}{4(1+c)}. \end{aligned} \tag{16}$$

The drag method failed to locate the TS of this PES, and the details can be seen in [17]. The starting point O selected is tentatively far from the TS but close to one local minimum. We test five different searching directions *OA*, *OB*, *OC*, *OD,* and *OE*, as indicated in Fig. 5. For the PFR method, only two trajectories with *OC* and *OD* as searching directions reach the TSs successfully. While for the EFR method, all five searching directions considered converge eventually to the TSs. Compared to the drag method, the robustness of the FR method is evident. The different searching directions may lead to different TSs because there are two saddle points available on the PES. In this case, it is necessary to test different initial searching directions to guarantee the lowest TS found.

The proposed FR algorithm is implemented in a first-principles total energy calculation package, and we describe below several prototype surface processes in which the forces are calculated explicitly using VASP. We first studied the oxygen diffusion on Cu(111) surface from a fcc hollow site to the neighbor hcp hollow site. The Cu(111) surface is modeled using a five-layer slab with nine atoms per layer, and the oxygen atom and metal atoms in top three layers are fully relaxed. For this system, the direction of the MEP pointing straightforward from the fcc site to hcp site is denoted as $PM'$ in Fig. 6a. The searching direction is *PM,* and the angle between *PM* and $PM'$ is $\theta$. Starting from a point near to fcc site, we search the TS using PFR, EFR, and dimer methods, respectively. The number of iterations to reach the TS at different $\theta$ is shown in Fig. 7. It is found that regardless of $\theta$, the number of iterations for the FR method is much less than that of the dimer method, indicating that the FR method is 2–4 times faster than the dimer method.

It should be noted that the TS located by the PFR method at $\theta = 45°$ is not the targeted TS but a neighboring equivalent TS, while for the EFR method, the target TS is always found for all angles considered. This suggests that the EFR method is more reliable. In addition, for all the cases except the PFR method at $\theta = 45°$, the located TSs by the FR method and the dimer method are exactly same and the corresponding structure is shown in Fig. 6b. Moreover, it can be seen from Fig. 7 that compared to the PFR method and the dimer method, the number of iterations required for the EFR method is almost independent on $\theta$, which demonstrates the robustness of EFR method again. From the optimized TS, it is convenient to obtain the IS (fcc site) and FS (hcp site) using the IRC approach. The barrier is calculated to be 0.37 eV with respect to the fcc site, which agrees well with the literature (0.40 eV [27] or 0.45 eV [28]), and the difference can be ascribed to the different computational parameters.

We are now in a position to address $O_2$ dissociation on Cu(111), which is a typical elementary reaction step occurred in various oxidation reaction on transition metal surfaces. Cu(111) surface was modeled using a five-layer

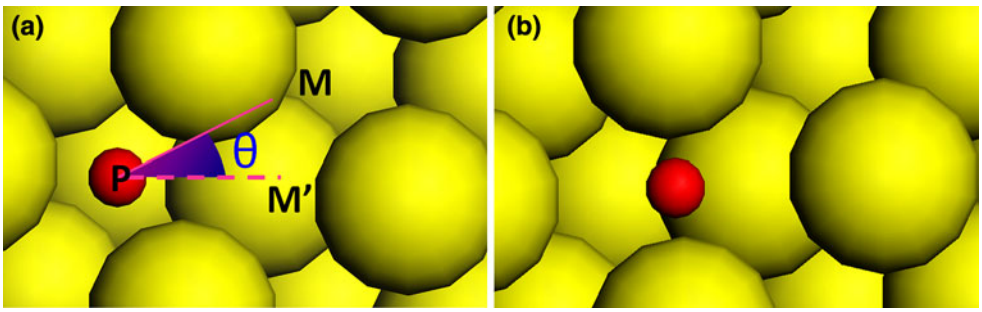


**Fig. 6** (Colored on line) The structures for oxygen diffusion on the Cu(111) surface at the initial state (**a**) and the optimized transition state (**b**). The *yellow balls* are Cu atoms, and the red one denotes oxygen atom. $PM'$ is the direction of MEP, and $PM$ is the initial searching direction. *Black circle* is the angle between $PM$ and $PM'$

slab with nine atoms per layer (oxygen coverage is 2/9 ML), and the oxygen atoms and metal atoms in top three layers were fully relaxed. For this process, the stable FS, namely the dissociated two oxygen atoms locating in the neighboring fcc sites of Cu(111), is more or less well defined. However, there are a number of possible configurations for $O_2$ adsorption on the surface with similar energies; therefore, the selection of the IS is a bit arbitrary. Since both the IS and the FS are required in (CI-)NEB or LST/QST method, this would make the location of the TS time-consuming and may even lead to the different TS.

Using the direction of O–O bond as the initial searching direction (black arrow in Fig. 8a for the initial searching direction) and the well-defined FS as the starting point, the EFR method locates the TS (Fig. 8b) after 24 iterations, while the dimer method reaches the same TS after 156 iterations with the same searching direction and starting point. The EFR method is 6.5 times faster than the dimer method. Using the IRC approach, the IS (Fig. 8c) can be obtained directly. The corresponding barrier for dissociation is 0.06 eV with respect to the IS and 2.36 eV with respect to the FS. The bond length of oxygen molecule at the TS is 1.67 Å. From the literature, the calculated barrier at the coverage of ½ ML is 0.2 eV with respect to the IS and 2.6 eV with respect to the FS [28], and the experimental value varies in the range of 0.07–0.17 eV [29]. Since the stronger repulsion between neighboring $O_2$ at higher coverage would result in a higher barrier, our results agree well with previous calculations and experiments.

Finally, a more complex reaction of $CH_3 + O \rightarrow CH_3O$ on Rh(111) is investigated. The Rh(111) surface is modeled using a five-layer slab with four atoms per layer, and the adsorbates and the top three layers were allowed to relax. For this reaction, though the formation of the C–O bond is essential, the displacement of the methyl group at the TS is significant and cannot be neglected. Namely, C–O bond significantly departs away from the reaction coordinate and could not be the proper reaction coordinate. This can be seen clearly from the vibration mode corresponding

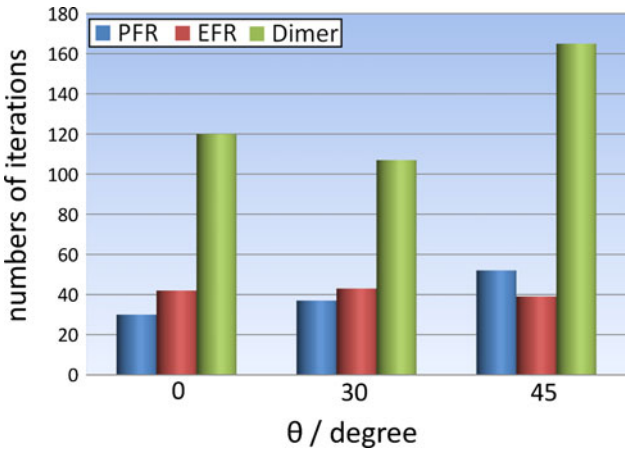


**Fig. 7** (Colored on line) The dependence of the number of iterations to locate the TS with different methods on $\theta$. $\theta$ is the angle between $PM$ and $PM'$ as indicated in Fig. 6

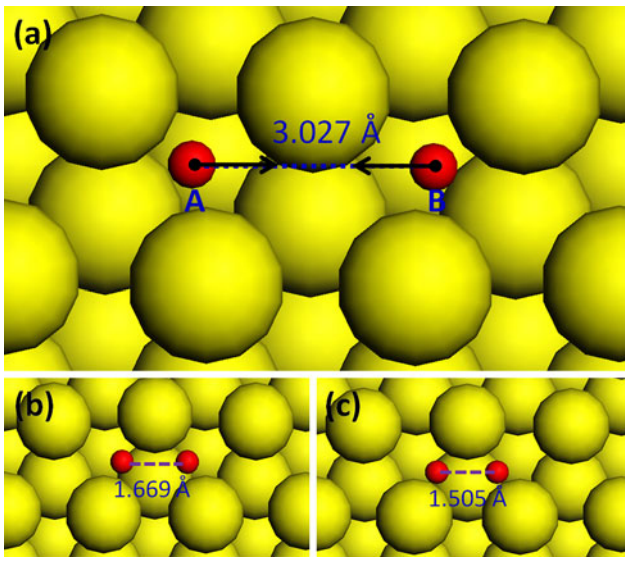


**Fig. 8** (Colored on line) $O_2$ dissociation on the Cu(111) surface at the final state (**a**), the transition state (**b**), and the initial state (**c**). The *black arrows* show the searching direction. The *yellow* and *red balls* are Cu and O atoms, respectively

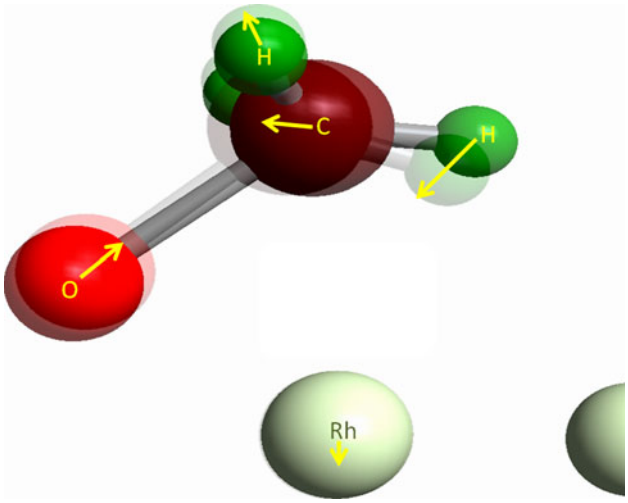


**Fig. 9** (Colored on line) The identified TS and the reaction coordinate (the vibration mode of the imaginary frequency) for the reaction $CH_3 + O \rightarrow CH_3O$ on Rh(111) surface. The *yellow arrows* give the directions of the MEP at the optimized TS

to the imaginary frequency at the optimized TS (see Fig. 9). Using the C–O bond as the initial searching direction and starting from the IS, the PFR method fails to reach the TS even after a thousand of iterations. In contrast, the EFR method succeeds to find the TS after 264 iterations. Using the same starting point and initial searching direction, the dimer method reaches the same TS after 245 iterations. At the TS, the calculated barrier is 1.25 eV, and the C–O bond length is 1.87 Å.

For this example, the EFR method has the almost same efficiency as the superlinearly converging dimer method. It should be noted that the optimizer used in the dimer is limited memory formulation of the Broyden–Fletcher–Goldfarb–Shanno optimization (L-BFGS), which converges much faster than conjugate gradient and steepest descent methods [26]. Nevertheless, the similar efficiency of the EFR algorithm using the slow steepest descent algorithm and the dimer method using advanced optimizer indicates that the EFR method is highly efficient for locating the TS. Part of the reasons is that two images are included to judge the searching direction using the dimer methods, whereas only one image is required for the force reversed method. We expect that the combination of EFR method with more advanced optimizer would further improve the efficiency of the proposed algorithm.

## 4 Conclusions

We proposed a simple, efficient, and robust force reversed method to search the transition states without the detailed knowledge of the initial state and final state, as required typically in other algorithms such as (Ci)NEB and LST/QST. The present algorithm requires only a rough or even "bad" initial searching direction. More important, only single image calculation is necessary for the searching of TS as a "normal structure optimization." Compared to the other methods that require multiple images, the present algorithm saves significantly the computational cost. The proposed algorithm has been applied successfully to various prototype reactions such as adatom diffusion, bond breaking, and making processes. We found that the force reversed method converges efficiently without losing the accuracy comparing to the dimer method. Depending on the system, the enhanced force reversed algorithm is similar or even faster than the superlinearly converging dimer method.

**Acknowledgments** Project supported by the National Natural Science Foundation of China (Grant No. 21103165, 20873142, 20733008).

## References

1. Hratchian HP, Schlegel HB (2005) In: Dykstra C, Frenking G, Kim K, Scuseria G (eds) Finding minima transition states and following reaction pathways on ab initio potential energy surfaces in theory and application of computational chemistry: the first forty years. Elsevier, Amsterdam
2. Sun JQ, Ruedenberg K (1994) J Chem Phys 101:2157
3. Culot P, Dive G, Nguyen VH, Ghuysen JM (1992) Theor Chim Acta 82:189
4. Cerjan CJ, Miller WH (1981) J Chem Phys 75:2800
5. Maeda S, Ohno K, Morokuma K (2009) J Phys Chem A 113:1704
6. Michaelides A, Hu P, Alavi A (1999) J Chem Phys 111:1343
7. Wang HF, Liu ZP (2008) J Am Chem Soc 130:10996
8. Bofill JM, Anglada JM (2001) Theor Chem Acc 105:463
9. Quapp W, Hirsch M, Imig O, Heidrich D (1998) J Computat Chem 19:1087
10. Liu ZP, Hu P (2004) Top Catal 28:71
11. Halgren TA, Lipscomb WN (1977) Chem Phys Lett 49:225
12. Govind N, Petersen M, Fitzgerald G, King-Smith D, Andzelm J (2003) Comput Mater Sci 28:250
13. Ren WEW, Vanden-Eijnden E (2002) Phys Rev B 66:052301
14. Jónsson H, Mills G, Jacobsen KW (1998) In: Berne BJ, Ciccotti G, Coker DF (eds) Nudged elastic band method for finding minimum energy paths of transitions in classical and quantum dynamics in condensed phase simulations. World Scientific, Singapore
15. Henkelman G, Uberuaga BP, Jónsson H (2000) J Chem Phys 113:9901
16. Henkelman G, Jónsson H (1999) J Chem Phys 111:7010
17. Henkelman G, Jóhannesson G, Jónsson H (2000) In: Schwartz SD (ed) Methods for finding saddle points and minimum energy paths in progress on theoretical chemistry and physics. Kluwer Academic, New York
18. Rothman MJ, Lohr LL (1980) Chem Phys Lett 70:405
19. Bitzek E, Koskinen P, Gähler F, Moseler M, Gumbsch P (2006) Phys Rev Lett 97:170201
20. Fukui K (1981) Acc Chem Res 14:363
21. Kresse G, Hafner J (1993) Phys Rev B 48:13115

22. Perdew JP, Burke K, Wang Y (1996) Phys Rev B 54:16533
23. Blöchl PE (1994) Phys Rev B 50:17953
24. Kresse G, Joubert J (1999) Phys Rev B 59:1758
25. Eckert F, Werner HJ (1998) Theor Chem Acc 100:21
26. Kästner J, Sherwood P (2008) J Chem Phys 128:014106
27. Soon A, Todorova M, Delley B, Stampfl C (2006) Phys Rev B 73:165424
28. Xu Y, Mavrikakis M (2001) Surf Sci 494:131
29. Habraken FHPM, Kieffer EPh, Bootsma GA (1979) Surf Sci 83:45